Acta Crystallographica Section D
Biological Crystallography
ISSN 0907-4449

The IMAGINE instrument: first neutron protein structure and new capabilities for neutron macromolecular crystallography

Flora Meilleur,[a,b]* Parthapratim Munshi,[b,c] Lee Robertson,[b] Alexandru D. Stoica,[b] Lowell Crow,[b] Andrey Kovalevsky,[b] Tibor Koritsanszky,[b] Bryan C. Chakoumakos,[b] Robert Blessing[d] and Dean A. A. Myles[b]

[a]Department of Molecular and Structural Biochemistry, NCSU, Raleigh, NC 27695, USA, [b]Neutron Sciences Directorate, ORNL, Oak Ridge, TN 37831, USA, [c]Department of Chemistry, MTSU, Murfreesboro, TN 37132, USA, and [d]Hauptman–Woodward Medical Research Institute, Buffalo, NY 14203, USA

Correspondence e-mail: meilleurf@ornl.gov

Received 13 May 2013
Accepted 15 July 2013

PDB Reference: perdeuterated rubredoxin, 4k9f

The first high-resolution neutron protein structure of perdeuterated rubredoxin from *Pyrococcus furiosus* (*Pf*Rd) determined using the new IMAGINE macromolecular neutron crystallography instrument at the Oak Ridge National Laboratory is reported. Neutron diffraction data extending to 1.65 Å resolution were collected from a relatively small 0.7 mm^3 *Pf*Rd crystal using 2.5 d (60 h) of beam time. The refined structure contains 371 out of 391, or 95%, of the D atoms of the protein and 58 solvent molecules. The IMAGINE instrument is designed to provide neutron data at or near atomic resolution (1.5 Å) from crystals with volume <1.0 mm^3 and with unit-cell edges <100 Å. Beamline features include novel elliptical focusing mirrors that deliver neutrons into a 2.0 × 3.2 mm focal spot at the sample position with full-width vertical and horizontal divergences of 0.5 and 0.6°, respectively. Variable short- and long-wavelength cutoff optics provide automated exchange between multiple-wavelength configurations (λ_{min} = 2.0, 2.8, 3.3 Å to λ_{max} = 3.0, 4.0, 4.5, ∼20 Å). These optics produce a more than 20-fold increase in the flux density at the sample and should help to enable more routine collection of high-resolution data from submillimetre-cubed crystals. Notably, the crystal used to collect these *Pf*Rd data was 5–10 times smaller than those previously reported.

1. Introduction

While atomic-level understanding of biological structure and function has come largely from NMR and X-ray crystallography, H atoms, which constitute ∼50% of the atoms in proteins and scatter X-rays weakly, can only be seen (if at all) in crystal structures determined to ultrahigh resolutions of <1.0 Å. However, many H atoms remain invisible even at ultrahigh resolution owing to their mobility. Thus, in many cases reliable structural information on protein and water H atoms is missing, precluding more detailed fundamental analyses and leaving specific questions concerning ligand recognition and binding, catalytic mechanism and protein hydration unanswered.

Neutron crystallography can locate H-atom positions in biological structures at moderate resolutions of 1.5–2.2 Å. This is because neutrons are scattered by atomic nuclei, rather than by electrons, and consequently the neutron scattering length does not depend on the atomic number. The neutron scattering lengths of hydrogen and deuterium are similar to those of the 'heavy' atoms carbon, oxygen and nitrogen, and both H and D atoms are readily visualized in neutron-density maps calculated from neutron diffraction data. This is beneficial for determining the protonation states of catalytic residues in enzymes (Coates *et al.*, 2008; Blakeley *et al.*, 2008; Adachi *et al.*, 2009; Glusker *et al.*, 2010; Tomanicek *et al.*, 2011; Fisher *et al.*, 2012; Kovalevsky *et al.*, 2012) and hydrogen-bonding patterns and ligand-binding interactions in proteins, and, as complete D_2O water molecules are prominent in neutron-density maps, for detailed analysis of the structure and dynamics of water in hydration layers at the protein–solvent interface (Bon *et al.*, 1999; Blakeley *et al.*, 2004; Fisher *et al.*, 2012; Chen *et al.*, 2012). Moreover, since the neutrons used in the crystallographic experiments are uncharged and have thermal energies of just a few meV, neutron diffraction does not cause radiation-damage effects in protein crystals and structures are

routinely determined at room temperature, free from the radiation-induced damage and artifacts that can be of concern in X-ray crystallography.

Despite these advantages, the broader use of neutron diffraction analysis has been restricted by the limited availability and flux of neutron beams and by the time required to collect data from small or weakly scattering samples. The development of neutron image-plate detector systems (Niimura, 1999), cylindrical detector designs (Tanaka *et al.*, 2002) and the use of 'white-beam' Laue diffraction geometry (Cipriani *et al.*, 1996; Niimura *et al.*, 1997) have provided 10–100-fold gains in data-collection rates at neutron reactors (Myles *et al.*, 1997; Cole *et al.*, 2001) and have reduced data-collection times to days or hours for perdeuterated samples (Munshi *et al.*, 2012). A new generation of neutron macromolecular crystallography instruments are now coming on-line at facilities worldwide, namely the upgraded LADI-III instrument at the ILL in France (Blakeley *et al.*, 2010), the iBiX instrument at JSNS in Japan (Tanaka *et al.*, 2010), the BioDiff instrument at FRM-2 in Germany and the TOPAZ (Frost *et al.*, 2010; Zikovsky *et al.*, 2011), MaNDi (Schultz *et al.*, 2005; Coates *et al.*, 2010) and IMAGINE instruments at the Oak Ridge National Laboratory (ORNL), USA. Here, we briefly outline the design features and performance of the newest of these facilities, IMAGINE, report the first high-resolution neutron protein structure determined on the beamline and provide a benchmark comparison of the same structures from other neutron beamlines.

2. The IMAGINE instrument

ORNL operates two powerful neutron sources for neutron scattering research: the Spallation Neutron Source (SNS), which currently provides the most intense pulsed neutron beams in the world, and the 85 MW High Flux Isotope Reactor (HFIR), which currently provides one of the highest steady-state neutron fluxes in the world. The HFIR was recently equipped with a high-performance cold neutron source that has a brightness of 1.6×10^{13} neutrons cm^{-2} s^{-1} sr^{-1} Å^{-1} at the peak (λ = 2.6 Å) and delivers neutrons to a new suite of instruments that are optimized for structural biology and materials research (Lynn *et al.*, 2006; Crow *et al.*, 2011; Wignall *et al.*, 2012; Taniguchi *et al.*, 2013).

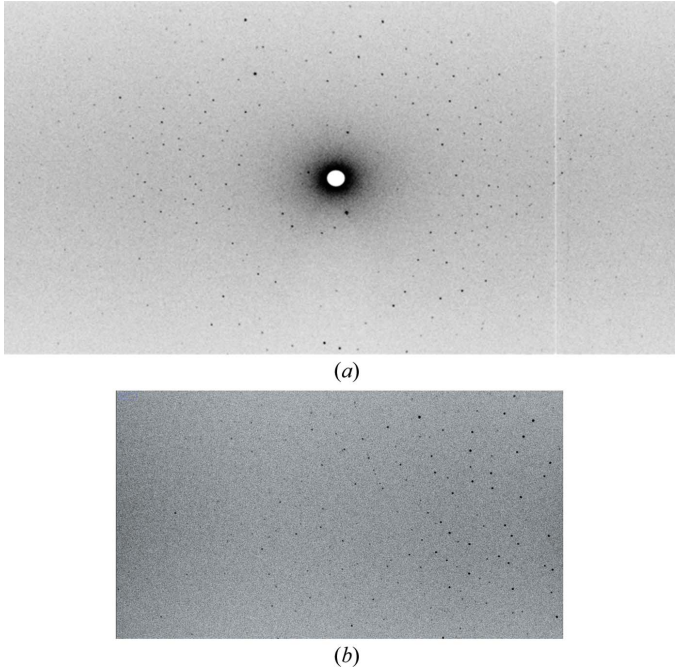

(*a*)

(*b*)

Figure 1
(*a*) Typical quasi-Laue diffraction pattern of *Pf*Rd (5 h exposure); (*b*) high-resolution reflections.

The IMAGINE diffractometer is designed for the rapid collection (hours to days) of high-resolution (~1.5 Å) Laue or quasi-Laue data from small single crystals (<1.0 mm^3) of moderate unit-cell size (~100 Å). The instrument sits on the end-station of cold guide CG-4, which has a flux of 2×10^9 neutrons s^{-1} cm^{-2} over the useful 2–10 Å wavelength range. The instrument receives neutrons from a 19×12 mm^2 section of the CG-4 guide. The neutron wavelength and bandpass delivered to the sample is varied by automated exchange of three neutron mirrors and three pairs of neutron filters that provide short-wavelength (λ_{min} = 2.0, 2.8 and 3.3 Å) and long-wavelength (λ_{max} = 3.0, 4.0 and 4.5 Å) cutoffs, respectively. A pair of elliptically shaped mirrors then collects and focuses the resulting beam vertically and horizontally down to 2×3.2 mm^2 at the sample position, with full-width vertical and horizontal divergences of 0.5 and 0.6°, respectively. This results in a more than 20-fold increase in flux density at the sample position. Additional collimation and beam-defining apertures can be placed after the elliptical mirrors to reduce divergence and to match the beam size to the sample. The diffractometer uses a cylindrical neutron image-plate design (Niimura *et al.*, 1994; Cipriani *et al.*, 1996) that is available commercially from MAATEL. A more detailed description of the beamline neutronics, optics and instrument performance at each wavelength configuration will be reported separately (Meilleur *et al.*, in preparation)

3. Case study: deuterated *Pyrococcus furiosus* rubredoxin

P. furiosus is an anaerobic sulfur-reducing species of archaea. It exhibits optimum growth near 373 K. *P. furiosus* rubredoxin (*Pf*Rd) is a 53-amino-acid protein containing an Fe atom bound to the S atoms of four cysteine residues in a nearly regular tetrahedron. Rubredoxins are involved in electron transfer (Lovenberg & Sobel, 1965). *Pf*Rd has a long history as a crystallographic test system (Bau *et al.*, 1998; Mukherjee, 1999; Bau, 2004; Li *et al.*, 2004; Weiss *et al.*, 2008; Gardberg *et al.*, 2010; Munshi *et al.*, 2012) and is of interest for its remarkable high-temperature stability.

3.1. Expression and crystallization of perdeuterated *Pf*Rd

A pET24d expression vector harboring the *Pf*Rd gene, a gift from Michael Adams and Frank Jenney at the University of Georgia, was transformed into *Escherichia coli* strain BL21 (DE3). The cells were adapted for growth in deuterated minimal medium (Meilleur *et al.*, 2004) and perdeuterated *Pf*Rd was expressed in high yield using fermentation protocols (Meilleur *et al.*, 2009). Large perdeuterated *Pf*Rd crystals were grown as described previously (Bau *et al.*, 1998; Gardberg *et al.*, 2010).

3.2. Data collection and reduction

A relatively small 0.7 mm^3 *Pf*Rd crystal was selected and mounted in a quartz capillary for data collection at room temperature. Quasi-Laue data were collected using a narrow-bandpass 2.8–4.0 Å optical configuration ($\lambda_{peak} \simeq 3.5$ Å, $d\lambda/\lambda \simeq 35\%$) that delivers 3×10^7 neutrons cm^{-2} s^{-1} at the sample position. The data extended to 1.65 Å resolution after ~5 h exposure (Fig. 1). A total of 12 images were collected at 10° step intervals to give a total exposure time of 60 h. Laue images were measured, indexed and integrated using the *LAUEGEN* suite of programs from *CCP*4 (Helliwell *et al.*, 1989; Campbell *et al.*, 1998), wavelength-normalized to account for the

Table 1
Neutron data-collection and refinement statistics for rubredoxin.

Values in parentheses are for the highest resolution shell.

Instrument	IMAGINE	LADI-III	LADI-III	BIX-3	PCS	D19
PDB code	4k9f†	3kyx‡	3rzt§	1vcx¶	N/A††	4ar3‡‡
Crystal volume (mm^3)	0.7	3.9	3.2	5.0	4.0	6.9
Data-collection time (h)	60	118	14	840	108	192
H or D	D	D	D	H/D	H/D	D
Maximum resolution (Å)	1.75	1.68	1.75	1.5	2.1	1.27
R_{merge} (%)	12.7 (18.5)	9.5 (9.9)	15.3 (18.9)	9.6 (23.2)	12.5 (23.6)	8.3 (75.4)
$R_{p.i.m.}$ (%)	7.1 (13.1)	4.0 (8.6)	7.2 (11.5)	N/A	N/A	4.5 (49.3)
Mean $I/\sigma(I)$	7.0 (3.7)	14.9 (4.1)	8.4 (3.6)	8.5 (3.1)	3.7 (2.1)	10.1 (1.6)
Completeness (%)	76.4 (54.1)	82.3 (34.0)	75.6 (56.2)	81.9 (53.1)	69.6 (62.8)	93.0 (88.2)
Multiplicity	3.5 (2.2)	6.1 (1.4)	4.6 (2.6)	N/A	(2.5)	3.1 (2.3)
R_{work} (%)	19.8	24.8	20.22	18.6	N/A	19.9
R_{free} (%)	24.1	26.7	24.90	21.7	N/A	23.8
R.m.s.d., bond lengths (Å)	0.013	0.005	0.013	0.010	N/A	0.023
R.m.s.d., angles (°)	0.994	0.969	1.257	1.242	N/A	1.956
Protein H/D atoms (%)	95	97	94	94	N/A	99
Solvent molecules	58	28	37	37	N/A	149

† Present work: resolution range 27.14–1.75 (1.84–1.75) Å, Total No. of reflections observed 14 484 (895), No. of unique reflections 4095 (410), average B factors 20.5 Å^2 (protein), 14.7 Å^2 (metal ion), 32.1 Å^2 (water). ‡ Gardberg *et al.* (2010). § Munshi *et al.* (2012). ¶ Kurihara *et al.* (2004). †† Li *et al.* (2004). ‡‡ Cuypers *et al.* (2013).

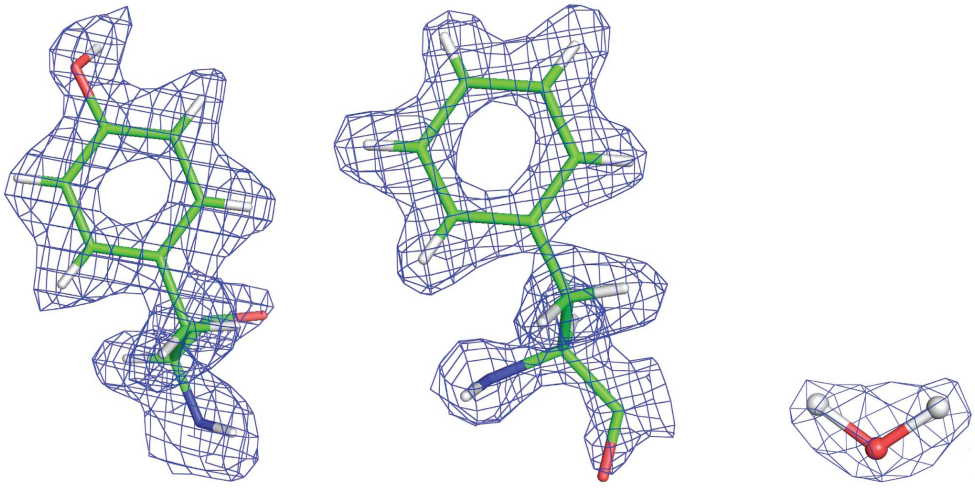

Figure 2
Neutron-density maps ($2F_o - F_c$) at 1.5σ for the side chains of (*a*) Tyr12 and (*b*) Phe48 and (*c*) for D_2O

spectral distribution of the quasi-Laue beam using *LSCALE* (Arzt *et al.*, 1999) and then scaled and merged using *SCALA* (Winn *et al.*, 2011).

4. Results

The crystal belonged to space group $P2_12_12_1$, with unit-cell parameters a = 33.82, b = 34.80, c = 43.35 Å. Neutron data-collection and refinement statistics are summarized in Table 1. Whilst reflections in the last resolution shell (1.75–1.65 Å) were strong [40% complete with an $\langle I/\sigma(I)\rangle$ of 3.4], these data were excluded from the final data set because of the relatively low completeness in this shell. The resolution of the last shell for which the data completeness exceeded 50% was 1.84–1.75 Å [with 54% of reflections having $I/\sigma(I) > 3.7$]. The final model refined to values of R_{work} = 19.8%, R_{free} = 24.1% using *phenix.refine* (Adams *et al.*, 2010). A total of 371 out of 391, or 95%, of the D atoms of the protein were located in the neutron-density maps (Figs. 2*a* and 2*b*). A total of 58 heavy-water molecules were included in the final structure. Of these, 33 were assigned as full D_2O molecules with the characteristic 'boomerang' neutron density (Fig. 2*c*), a further 16 had 'stick' density for the O and one D atom and the remaining nine water molecules displayed only spherical neutron density. This can be compared with a total of 37 hydration waters modeled in the 1.5 Å resolution neutron structure of H/D-exchanged rubredoxin (Kurihara *et al.*, 2004), of which 15 had all three atoms fully located.

5. Discussion

The 1.75 Å resolution limit and the quality of the data collected from this 0.7 mm^3 *Pf*Rd crystal are similar to those for the data previously collected using larger crystals (∼3–4 mm^3; Kurihara *et al.*, 2004; Li *et al.*, 2004; Gardberg *et al.*, 2010; Munshi *et al.*, 2012; Myles *et al.*, 2012; Cuypers *et al.*, 2013; see Table 1). The R_{work} values for the refined structures are all similar. The fraction of protein H/D atoms reported in these structures varies from 92 to 96%. The number of water molecules located in the neutron-density maps of the three earlier structures varies between 28 and 37. Here, we have been able to assign an additional 21 water molecules based upon neutron density. While the precise function of rubredoxin is unknown, these additional water molecules contribute to a more complete model of the hydrogen-bonding interactions at the protein–solvent interface. Yet larger *Pf*Rd crystals of up to ∼7.0 mm^3 have recently been used to extend the neutron resolution to 1.3 Å and the refinement revealed 149 water positions and 99% D atoms for the protein (Cuypers *et al.*, 2013). These authors modeled four solvent molecules as hydroxonium ions in chemically unusual positions in the protein. Interestingly, in our structure only two of these solvent molecules are present and both are best modeled as D_2O.

6. Conclusion

Neutron diffraction has unique potential for scientific research and discovery, but remains a beam-intensity limited technique that is further constrained by the limited number of available neutron beamlines. The performance of the novel beam-focusing and wavelength-selection optics on IMAGINE meet all design goals and the improved flux density should enable the more routine collection of high-resolution data from submillimetre-cubed crystals. IMAGINE therefore adds new world-class capabilities and additional capacity to the world's growing suite of neutron macromolecular crystallography instruments and complements the design specifications of the SNS

TOPAZ and MaNDi instruments that are optimized for small-molecule and macromolecular crystallography, respectively. Increasing capacity, shortening data-collection times and reducing the requirement for crystal size below the critical 1 mm^3 threshold will help to extend the range, scale and complexity of problems that are accessible to neutron analysis.

We thank Kevin L. Weiss and Junhong He for their support with the production of deuterated rubredoxin at ORNL's Center for Structural Molecular Biology, which is supported by the US Department of Energy's Office of Biological and Environmental Research. Research conducted at ORNL's High Flux Isotope Reactor was sponsored by the Scientific User Facilities Division, Office of Basic Energy Sciences, US Department of Energy. The IMAGINE project is partially supported by the National Science Foundation under grant No. 0922719.

References

Adachi, M. *et al.* (2009). *Proc. Natl Acad. Sci. USA*, **106**, 4641–4646.
Adams, P. D *et al.* (2010). *Acta Cryst.* D**66**, 213–221.
Arzt, S., Campbell, J. W., Harding, M. M., Hao, Q. & Helliwell, J. R. (1999). *J. Appl. Cryst.* **32**, 554–562.
Bau, R. (2004). *J. Synchrotron Rad.* **11**, 76–79.
Bau, R., Rees, D. C., Kurtz, D. M. Jr, Scott, R. A., Huang, H., Adams, M. W. W. & Eidsness, M. K. (1998). *J. Biol. Inorg. Chem.* **3**, 484–493.
Blakeley, M. P., Kalb, A. J., Helliwell, J. R. & Myles, D. A. A. (2004). *Proc. Natl Acad. Sci. USA*, **101**, 16405–16410.
Blakeley, M. P., Ruiz, F., Cachau, R., Hazemann, I., Meilleur, F., Mitschler, A., Ginell, S., Afonine, P., Ventura, O. N., Cousido-Siah, A., Haertlein, M., Joachimiak, A., Myles, D. & Podjarny, A. (2008). *Proc. Natl Acad. Sci. USA*, **105**, 1844–1848.
Blakeley, M. P., Teixeira, S. C. M., Petit-Haertlein, I., Hazemann, I., Mitschler, A., Haertlein, M., Howard, E. & Podjarny, A. D. (2010). *Acta Cryst.* D**66**, 1198–1205.
Bon, C., Lehmann, M. S. & Wilkinson, C. (1999). *Acta Cryst.* D**55**, 978–987.
Campbell, J. W., Hao, Q., Harding, M. M., Nguti, N. D. & Wilkinson, C. (1998). *J. Appl. Cryst.* **31**, 496–502.
Chen, J. C., Hanson, B. L., Fisher, S. Z., Langan, P. & Kovalevsky, A. Y. (2012). *Proc. Natl Acad. Sci. USA*, **109**, 15301–15306.
Cipriani, F., Castagna, J. C., Wilkinson, C., Lehmann, M. S. & Büldt, G. (1996). *Basic Life Sci.* **64**, 423–431.
Coates, L., Stoica, A. D., Hoffmann, C., Richards, J. & Cooper, R. (2010). *J. Appl. Cryst.* **43**, 570–577.
Coates, L., Tuan, H.-F., Tomanicek, S., Kovalevsky, A., Mustyakimov, M., Erskine, P. & Cooper, J. (2008). *J. Am. Chem. Soc.* **130**, 7235–7237.
Cole, J. M., McIntyre, G. J., Lehmann, M. S., Myles, D. A. A., Wilkinson, C. & Howard, J. A. K. (2001). *Acta Cryst.* A**57**, 429–434.
Crow, L., Robertson, L., Bilheux, H., Fleenor, M., Iverson, E., Tong, X., Stoica, D. & Lee, W. (2011). *Nucl. Instrum. Methods Phys. Res. A*, **634**, S71–S74.
Cuypers, M. G., Mason, S. A., Blakeley, M. P., Mitchell, E. P., Haertlein, M. & Forsyth, V. T. (2013). *Angew. Chem. Int. Ed.* **52**, 1022–1025.
Fisher, S. Z., Aggarwal, M., Kovalevsky, A. Y., Silverman, D. N. & McKenna, R. (2012). *J. Am. Chem. Soc.* **134**, 14726–14729.
Frost, M., Hoffmann, C., Thomison, J., Overbay, M., Austin, M., Carman, P., Viola, R., Miller, E. & Mosier, L. (2010). *J. Phys. Conf. Ser.* **251**, 012084.
Gardberg, A. S., Del Castillo, A. R., Weiss, K. L., Meilleur, F., Blakeley, M. P. & Myles, D. A. A. (2010). *Acta Cryst.* D**66**, 558–567.
Glusker, J. P., Carrell, H. L., Kovalevsky, A. Y., Hanson, L., Fisher, S. Z., Mustyakimov, M., Mason, S., Forsyth, T. & Langan, P. (2010). *Acta Cryst.* D**66**, 1257–1261.
Helliwell, J. R., Habash, J., Cruickshank, D. W. J., Harding, M. M., Greenhough, T. J., Campbell, J. W., Clifton, I. J., Elder, M., Machin, P. A., Papiz, M. Z. & Zurek, S. (1989). *J. Appl. Cryst.* **22**, 483–497.
Kovalevsky, A., Hanson, B. L., Mason, S. A., Forsyth, V. T., Fisher, Z., Mustyakimov, M., Blakeley, M. P., Keen, D. A. & Langan, P. (2012). *Acta Cryst.* D**68**, 1201–1206.
Kurihara, K., Tanaka, I., Chatake, T., Adams, M. W. W., Jenney, F. E., Moiseeva, N., Bau, R. & Niimura, N. (2004). *Proc. Natl Acad. Sci. USA*, **101**, 11215–11220.
Li, X., Langan, P., Bau, R., Tsyba, I., Jenney, F. E., Adams, M. W. W. & Schoenborn, B. P. (2004). *Acta Cryst.* D**60**, 200–202.
Lovenberg, W. & Sobel, B. E. (1965). *Proc. Natl Acad. Sci. USA*, **54**, 193–199.
Lynn, G. W., Heller, W., Urban, V., Wignall, G. D., Weiss, K. & Myles, D. A. A. (2006). *Physica B*, **385–86**, 880–882.
Meilleur, F., Contzen, J., Myles, D. A. A. & Jung, C. (2004). *Biochemistry*, **43**, 8744–8753.
Meilleur, F., Weiss, K. L. & Myles, D. A. A. (2009). *Methods Mol. Biol.* **544**, 281–292.
Mukherjee, M. (1999). *Acta Cryst.* D**55**, 820–825.
Munshi, P., Chung, S.-L., Blakeley, M. P., Weiss, K. L., Myles, D. A. A. & Meilleur, F. (2012). *Acta Cryst.* D**68**, 35–41.
Myles, D. A. A., Bon, C., Langan, P., Cipriani, F., Castagna, J. C., Lehmann, M. S. & Wilkinson, C. (1997). *Physica B*, **241**, 1122–1130.
Myles, D. A. A., Dauvergne, F., Blakeley, M. P. & Meilleur, F. (2012). *J. Appl. Cryst.* **45**, 686–692.
Niimura, N. (1999). *Curr. Opin. Struct. Biol.* **9**, 602–608.
Niimura, N., Karasawa, Y., Tanaka, I., Miyahara, J., Takahashi, K., Saito, H., Koizumi, S. & Hidaka, M. (1994). *Nucl. Instrum. Methods Phys. Res. A*, **349**, 521–525.
Niimura, N., Minezaki, Y., Nonaka, T., Castagna, J. C., Cipriani, F., Høghøj, P., Lehmann, M. S. & Wilkinson, C. (1997). *Nature Struct. Biol.* **4**, 909–914.
Schultz, A. J., Thiyagarajan, P., Hodges, J. P., Rehm, C., Myles, D. A. A., Langan, P. & Mesecar, A. D. (2005). *J. Appl. Cryst.* **38**, 964–974.
Tanaka, I., Kurihara, K., Chatake, T. & Niimura, N. (2002). *J. Appl. Cryst.* **35**, 34–40.
Tanaka, I., Kusaka, K., Hosoya, T., Niimura, N., Ohhara, T., Kurihara, K., Yamada, T., Ohnishi, Y., Tomoyori, K. & Yokoyama, T. (2010). *Acta Cryst.* D**66**, 1194–1197.
Taniguchi, T., Kadowaki, H., Takatsu, H., Fak, B., Ollivier, J., Yamazaki, T., Sato, T. J., Yoshizawa, H., Shimura, Y., Sakakibara, T., Hong, T., Goto, K., Yaraskavitch, L. R. & Kycia, J. B. (2013). *Phys. Rev. B*, **87**, 06040.
Tomanicek, S. J., Wang, K. K., Weiss, K. L., Blakeley, M. P., Cooper, J., Chen, Y. & Coates, L. (2011). *FEBS Lett.* **585**, 364–368.
Weiss, K. L., Meilleur, F., Blakeley, M. P. & Myles, D. A. A. (2008). *Acta Cryst.* F**64**, 537–540.
Wignall, G. D., Littrell, K. C., Heller, W. T., Melnichenko, Y. B., Bailey, K. M., Lynn, G. W., Myles, D. A., Urban, V. S., Buchanan, M. V., Selby, D. L. & Butler, P. D. (2012). *J. Appl. Cryst.* **45**, 990–998.
Winn, M. D. *et al.* (2011). *Acta Cryst.* D**67**, 235–242.
Zikovsky, J., Peterson, P. F., Wang, X. P., Frost, M. & Hoffmann, C. (2011). *J. Appl. Cryst.* **44**, 418–423.